Published in final edited form as:
J Neural Eng. 2012 June ; 9(3): 036004. doi:10.1088/1741-2560/9/3/036004.

Recording evoked potentials during deep brain stimulation: development and validation of instrumentation to suppress the stimulus artefact

A R Kent[1] and **W M Grill**[1,2,3]

[1]Department of Biomedical Engineering, Duke University Durham, NC

[2]Department of Neurobiology, Duke University Durham, NC

[3]Department of Surgery Duke University Durham, NC

Abstract

Deep brain stimulation (DBS) is an effective treatment for movement disorders, but the selection of stimulus parameters is a clinical burden and often yields sub-optimal outcomes for patients. Measurement of electrically evoked compound action potentials (ECAPs) during DBS could offer insight into the type and spatial extent of neural element activation and provide a potential feedback signal for the rational selection of stimulus parameters and closed-loop DBS. However, recording ECAPs presents a significant technical challenge due to the large stimulus artefact, which can saturate recording amplifiers and distort short latency ECAP signals. We developed DBS-ECAP recording instrumentation combining commercial amplifiers and circuit elements in a serial configuration to reduce the stimulus artefact and enable high fidelity recording. We used an electrical circuit equivalent model of the instrumentation to understand better the sources of the stimulus artefact and the mechanisms of artefact reduction by the circuit elements. *In vitro* testing validated the capability of the instrumentation to suppress the stimulus artefact and increase gain by a factor of 1,000 to 5,000 compared to a conventional biopotential amplifier. The distortion of mock ECAP (mECAP) signals was measured across stimulation parameters, and the instrumentation enabled high fidelity recording of mECAPs with latencies of only 0.5 ms for DBS pulse widths of 50 to 100 μs/phase. Subsequently, the instrumentation was used to record *in vivo* ECAPs, without contamination by the stimulus artefact, during thalamic DBS in an anesthetized cat. The characteristics of the physiological ECAP were dependent on stimulation parameters. The novel instrumentation enables high fidelity ECAP recording and advances the potential use of the ECAP as a feedback signal for the tuning of DBS parameters.

1. Introduction

Deep brain stimulation (DBS) is a surgical therapy to treat medically refractory movement disorders, such as essential tremor (ET) [1,2] and Parkinson's disease (PD) [3], as well as other neurological disorders including epilepsy [4]. The DBS electrode is implanted in the ventral intermediate (Vim) nucleus of the thalamus for ET and the subthalamic nucleus (STN) or internal segment of the globus pallidus (GPi) for PD. An implantable pulse generator (IPG) is connected to the electrode via a subcutaneous wire and delivers high-frequency stimulation to the targeted brain region. Following implantation, the parameters of stimulation, including voltage, frequency, and pulse width are selected to produce symptom suppression.[5]

Address all correspondence to: Warren M. Grill, Ph.D. Duke University Department of Biomedical Engineering Hudson Hall, Rm 136 Box 90281 Durham, NC 27708-0281 warren.grill@duke.edu (919) 660-5276 Phone (919) 684-4488 Fax.

Current approaches to the selection of stimulation parameters are a significant clinical burden and often deprive patients of the optimal benefits of DBS. There are over 25,000 available combinations of stimulation voltage, frequency, and pulse width in a typical IPG (Medtronic Soletra 7426), but few data describing the relationships between stimulation parameters and clinical outcomes.[5] Further, because symptoms do not respond immediately or uniformly to DBS [6], it is not feasible to measure the steady-state symptom response to a wide range of stimulation parameters, as required to identify the most effective settings. The time course of response to DBS is on the order of seconds for ET [7], but minutes for bradykinesia in PD [6], making programming much more challenging for the latter. Moreover, it is unclear how to select parameters when there are no immediate or overt responses to stimulation, such as for epilepsy. Consequently, there are typically a large number of parameter adjustments necessary at follow-up visits, making programming time-consuming and costly [8], and many patients spend appreciable time with sub-optimal DBS treatment.[9,10]

Measuring neural activity during DBS may provide a means for rational selection of stimulation parameters. One strategy records ongoing EEG-like brain rhythms known as local field potentials (LFPs), which are μV-level signals reflecting synchronized neural activity.[11] For example, elevated theta oscillations (4–7 Hz) are observed within the thalamus of ET subjects at the characteristic frequency of pathological tremor [12], and elevated beta frequency power (13–35 Hz) is present within the STN and GPi of PD subjects [13]. LFPs are modulated following treatment with DBS, suggesting that clinical efficacy is dependent on the disruption of pathological synchronization.[14,15] However, a direct causal link between LFP activity measured during DBS and the corresponding motor symptoms has not yet been identified.[13]

We propose to record electrically evoked compound action potentials (ECAPs) during DBS, providing insight into the activity of neurons directly affected by stimulation. Each DBS pulse activates an ensemble of neurons near the electrode. Transmembrane currents generated during activation of individual neural elements create voltages that can be recorded from non-stimulating contacts on the DBS electrode. The characteristics of the ECAP are expected to depend on the type and spatial extent of neural element activation during DBS. The ECAP could thus provide signatures of clinical effectiveness that correspond to sufficient activation of the appropriate type(s) of neural elements [16], and could be used to tune stimulation parameters during DBS programming sessions. An analogous ECAP recording strategy has been used during cochlear nerve stimulation as a feedback signal for programming cochlear implants.[17,18] The ECAP could also be used as a feedback signal in closed-loop DBS systems that provide automated, periodic tuning of stimulation parameters to respond to patient needs.

The purpose of this study was to develop and evaluate instrumentation to record ECAPs during DBS. Recording the ECAP is challenging due to the large stimulus artefact that can cause amplifier saturation and mask the ECAP signal.[19,20] Available techniques to remove the stimulus artefact are inadequate for ECAP recording during DBS. Several techniques rely on signal processing strategies, including curve fitting [21], template subtraction [22], polarity averaging [23], and masker-probe paradigms [24]. Although several of these strategies have been used with some success in cochlear nerve ECAP recordings [24–26], they are performed after the amplification stage and thus limit the gain that can be used without amplifier saturation. Hardware methods are also used to reduce the artefact, including signal filtering for DBS-LFP recordings [19], which requires separation of the artefact and physiological signal in the frequency domain. Alternatively, sample-and-hold amplifiers [27] have enabled artefact-free recording from stimulating electrodes within

2 ms after the stimulation pulse [28,29], though have exhibited inconsistent performance. [30]

We sought to develop instrumentation that could reduce the artefact during the amplification stage and thereby enable high gain recording of ECAPs. The performance of this instrumentation was assessed through *in vitro* experiments, in which mock ECAPs were recorded in the presence of a stimulus artefact to characterize the input-output fidelity of the system. The instrumentation was then used to demonstrate that ECAPs could be recorded *in vivo* from the thalamus of the cat, with signal characteristics dependent on stimulation parameters. Finally, an electrical circuit equivalent model was developed to determine both the sources of the stimulus artefact recorded during the *in vitro* and *in vivo* experiments and the mechanisms of artefact reduction by the instrumentation. Preliminary results of this study were presented in a conference abstract.[31]

2. Methods

The design objective for the instrumentation was to make high fidelity ECAP recordings in the presence of a stimulus artefact. We used differential recordings from non-stimulating contacts on the DBS electrode to eliminate the need for additional recording electrodes and ensure that the recording contacts were near the neurons activated by stimulation. We sought to limit the artefact magnitude such that sufficient amplifier gain could be used without saturation, and to limit the artefact duration to avoid distorting short latency ECAPs. The DBS-ECAP instrumentation system combined battery-powered biopotential amplifiers in a serial configuration with diode clamps, amplifier blanking, and a relay at the stimulator. *In vitro* and *in vivo* experiments were conducted to characterize the ability of this instrumentation to limit the size of the stimulus artefact, enable higher gains without amplifier saturation, and record ECAPs with high fidelity.

2.1. In Vitro Experimental Setup

We used an *in vitro* setup to reproduce the experimental conditions of the DBS electrode within the brain (figure 1(a)). A DBS electrode was immersed in a saline bath (137 mM NaCl) and was used to deliver monopolar or bipolar stimulation, with two of the non-stimulating contacts connected to the recording system. Two DBS electrodes were tested: a clinical DBS electrode (Model 3387, Medtronic) and a custom mini DBS electrode (NuMed). The clinical DBS electrode had a lead body diameter of 1.27 mm, and four contacts of 1.5 mm height separated by 1.5 mm spacing. The mini DBS electrode, which was also used in the subsequent *in vivo* experiment, had a lead body diameter of 0.625 mm, and four contacts of 0.5 mm height separated by 0.5 mm spacing. Each DBS pulse triggered generation of a mock ECAP (mECAP), synthesized by a waveform generator (Model 33120A, Agilent) as a single cycle of sinusoidal current and delivered by a pair of tungsten microelectrodes near the DBS electrode. Given that power in the physiological ECAP frequency spectrum is confined to the 100 Hz to 4 kHz band, we used a 4 kHz mECAP sinusoid (0.25 ms duration), which would be most challenging to record with high fidelity due to the short signal duration. A helical stainless steel wire was used as the counter electrode for monopolar stimulation configurations, and a Ag/AgCl electrode (Model RE-5B, BASi) was used as the recording circuit reference. A custom program written in LabView (National Instruments) controlled delivery of DBS pulses, trigger pulses for the mECAP, timing of digital outputs to operate components in the DBS-ECAP instrumentation, and sampling of the signal (80 kHz sampling rate).

2.2. Testing Artefact Reduction and Recording Fidelity

Using the *in vitro* setup, we recorded the mECAP signal in the presence of a stimulus artefact across various stimulation parameters, DBS contact configurations, and recording system configurations. Charge-balanced, biphasic DBS was applied with clinically relevant stimulation parameters of 1 to 3 V amplitude, 50 to 500 μs/phase pulse width (symmetric and asymmetric pulses), 100 Hz frequency, and cathodic-phase first polarity. Three different contact configurations were used for stimulation and recording, with contacts designated 0-1-2-3 in the ventral-to-dorsal direction: monopolar stimulation with either symmetrical recording contacts (*monopolar symmetric*: 1+ stimulation, 0+/2− recording) or asymmetrical recording contacts (*monopolar asymmetric*: 0+ stimulation, 1+/2− recording), as well as bipolar stimulation (*bipolar*: 1+/2− stimulation, 0+/3− recording). The parameters for the mECAP were 0.1 to 2 ms latency and 0.1 to 0.5 mA peak-to-peak (P-P) input amplitude, which generated recorded amplitudes of 0.18 to 0.88 $mV_{P\text{-}P}$ in the monopolar symmetric configuration. We recorded these signals both with and without the circuit components used to suppress the artefact, as well as with a conventional setup using a single commercial biopotential amplifier (SR560, Stanford Research Systems). The extent of artefact reduction between recording systems was quantified by the change in amplifier gain that could be achieved without amplifier saturation and by distortion of the mECAP signal.

The signals recorded across these stimulation and recording conditions were analyzed to quantify mECAP distortion. For each trial, we collected a raw data set consisting of stimulus artefact and mECAP measurements for 10 s. Due to the small magnitude of the mECAPs, stimulus-triggered averaging was applied 64 times to improve the signal-to-noise ratio. The distortion of the recorded mECAP sinusoid was measured against an ideal sinusoidal voltage with the same duration and latency (accounting for phase shift), and with the ideal sinusoid magnitude fit using a least-squares approach. The sampling frequency of the ideal sinusoid was matched to that of the recorded sinusoid so that point-wise analysis could be performed. The magnitudes of both the ideal and recorded sinusoids were then normalized to the amplitude of the ideal sinusoid to avoid bias against larger magnitude mECAPs. Finally, distortion was measured as the root-mean square error between the magnitude-normalized recorded and ideal sinusoids. This value was divided by the number of samples in the sine wave to get an average distortion per sample (DPS) value. We defined *high fidelity recording* as having a DPS value < 0.5.

2.3. In Vivo Experimental Setup and ECAP Recording

We investigated the feasibility of recording *in vivo* ECAPs during thalamic DBS in an adult cat (figure 1(b)). Animal care and experimental procedures were reviewed and approved by the Institutional Animal Care and Use Committee of Duke University. The animal was initially anesthetized with ketamine HCl (35 mg/kg i.m.) and maintained with alpha chloralose (65 mg/kg i.v. supplemented at 15 mg/kg as needed). Artificial respiration maintained end tidal CO_2 at 3–4%, core temperature was maintained at 38°C with heating pads, arterial blood pressure was monitored with a catheter in the carotid artery, and fluids were continuously administered (10–15 ml/kg/hr).

The ventrolateral (VL) nucleus of the thalamus was targeted for implantation of the mini DBS electrode. The anesthetized cat lay prone with the head fixed in a stereotactic frame. Following a craniotomy, the VL thalamus was located using stereotactic technique [32,33] in conjunction with single-unit microelectrode recordings. Neurons in the dorsal region of the VL thalamus exhibited increased activity in response to passive movement of the contralateral hind limb.[33] Once the location of the VL thalamus was identified, a guide tube was inserted vertically into the brain using a micromanipulator, and the mini DBS electrode was inserted through the guide tube into the VL thalamus. To confirm that the

electrode was correctly placed in the VL thalamus, we recorded evoked responses from two contacts on the DBS electrode (0+/2−) during electrical stimulation of the contralateral sciatic nerve (biphasic pulses of 1 mA amplitude, 7 Hz frequency, and 50 μs pulse width).

The ECAP generated *in vivo* by DBS was measured across a range of clinically relevant stimulation parameters. Charge-balanced, biphasic DBS was applied at 1 to 3 V amplitude, 10 or 100 Hz frequency, 50 or 100 μs/phase pulse width, and both cathodic- and anodic-phase first polarities. The two contact configurations tested were monopolar symmetric (1+ stimulation, 0+/2− recording) and monopolar asymmetric (3+ stimulation, 2+/1− recording). A stainless steel retractor placed in the ipsilateral chest muscle acted as the counter electrode and a Ag/AgCl electrode (Model EL504, Biopac Systems) placed on the back of the neck was used as the reference electrode. To evaluate the performance of the instrumentation *in vivo*, we recorded ECAPs using the full DBS-ECAP instrumentation, after circuit components were removed from the instrumentation, and with the conventional amplifier setup. The animal was killed by intravenous injection of Euthasol (Virbac), and postmortem recordings were made at several time points to confirm the biological origin of the antemortem ECAPs. During all trials, ECAPs were recorded for 10 s, with trials separated by 10 s, and stimulus-triggered averaging was applied 64 times.

2.4. Histology

Following completion of ECAP recording, the anatomical location of the mini DBS electrode was determined. The electrode was removed and the animal was immediately perfused transcardially with saline followed by 10% formalin. The hemisphere of the brain containing the electrode path was excised and post-fixed in 10% formalin for 24 hours at 4°C. Subsequently, the tissue sample was placed in 30% sucrose at 4°C until it sank, cryoprotected with optimal cutting temperature compound (Tissue-Tek, Sakura), and frozen at −80°C.[34] The sample was cryosectioned into 50 μm coronal sections and mounted on glass slides. The sections were defatted and Nissl stained with 0.1% cresyl violet. Finally, the electrode track and nuclei of interest were identified at 2.5× magnification, such that the location of the electrode could be registered to a stereotactic atlas of the cat brain.[32]

2.5 Computational Model of the Stimulus Artefact

An electrical circuit equivalent model was developed, using PSpice (Cadence) and Comsol Script 1.2 (COMSOL) finite element modeling software, to study the sources of the stimulus artefact and mechanisms of artefact reduction by the recording instrumentation. The model included circuit representations of the DBS contact interface, saline or neural tissue medium, DBS voltage source, and components of the recording instrumentation (figure 2). The monopolar symmetric configuration was modeled in the electrical circuit equivalent simulations, with biphasic DBS delivered between contact 1 and a return electrode, and contacts 0 and 2 serving as inputs to the recording amplifier. The AC-coupled amplifier had a 100 MΩ, 25 pF parallel input impedance in series with a 0.1 μF capacitor at each input. The electrode-tissue interface at each DBS contact was represented as a parallel capacitance and resistance with values derived from literature [35], assuming biphasic DBS pulses of 1 mA amplitude.

The DBS contacts and return electrode were electrically interconnected by impedance representations of the saline or neural tissue medium. To calculate the bulk resistance of the medium, a three-dimensional model of the DBS electrode within a spherical volume conductor was developed in Comsol Script. The volume of the spherical conductor matched the approximate volume of the saline bath or cat skull, 3,502 or 524 cm^3, respectively. The saline and neural tissue were assumed to be homogenous, represented with volume conductivities (σ_V) of 2 S/m [36] and 0.3 S/m [37], respectively. The clinical or mini DBS

electrode was represented in the model with the appropriate geometrical dimensions, with contact 1 placed at the center of the volume conductor, and the conductivities of the DBS contacts and insulated shaft were 5×10^{6} S/m and 1×10^{-13} S/m, respectively.[38] A 1 V boundary condition was specified at one contact surface and the exterior boundary of the volume conductor was grounded. Comsol Script created a variable resolution mesh and solved the Poisson equation using the conjugate gradients method. The resistance was calculated using Ohm's law ($R = 1\ V / I_{norm}$), where I_{norm} was determined by integrating the normal current density over the contact surface. The resistance between two DBS contacts was calculated in a similar fashion, with the two contacts of interest set to ±0.5 V and the normal current density integrated across the positive contact surface.

The permittivity of the medium was incorporated into the circuit model by placing capacitors between the DBS contacts and return electrode, parallel to the volume conductor resistance.[39] Saline and neural tissue permittivity values were estimated from previous studies, having dielectric constants (K) of 75 (for 137 mM NaCl at DC) [40] and 1×10^{4} to 1×10^{6} (at frequencies below 1 kHz) [41,42], respectively. The permittivity (ε) was calculated as:

$$\varepsilon = K\varepsilon_0 \tag{1}$$

where ε_0 is the permittivity of free space (8.85×10^{-12} F/m). Subsequently, the bulk capacitance was calculated by assuming that the geometry of the DBS contact within the volume conductor was one of two concentric spherical conducting shells. The capacitance of this spherical capacitor was then calculated as:

$$C_V = 4\pi\varepsilon\frac{r_a r_b}{r_b - r_a} \tag{2}$$

where r_a and r_b are the radii of the DBS contact and volume conductor, respectively.[43] The radius used for the DBS contact was set such that the surface area of the spherical contact and actual cylindrical contact were matched, and the radius of the volume conductor was identical to that used in the Comsol Script model.

The circuit model was used to solve for the stimulus artefact voltage, measured across the amplifier inputs, resulting from DBS pulses of 3 V amplitude, 100 Hz frequency, 50 μs/phase pulse width, and cathodic-phase first polarity. Three models were constructed, in accord with the experiment studies: (i) an *in vitro* model, with the clinical DBS electrode in the saline bath, and (ii) an *in vivo* model, with the mini DBS electrode in neural tissue, and (iii) a postmortem *in vivo* model, with the mini DBS electrode in dead neural tissue. For the postmortem *in vivo* model, the dielectric constant K was reduced from the antemortem model by 2.7% [44], and the conductivity σ_V was reduced by 28% [45].

3. Results

We developed an instrumentation system to record ECAPs during DBS, evaluated the performance of the system through *in vitro* and *in vivo* experiments, and conducted analysis of an electrical circuit equivalent model to analyze the source of the stimulus artefacts and their reduction by the elements of the instrumentation.

3.1. Instrumentation Design

The DBS-ECAP instrumentation used three stages of series amplification and several circuit components to limit the stimulus artefact and enable high fidelity recording of short latency, small amplitude ECAP signals (figure 3(i)). Differential recordings were made from two

non-stimulating contacts on the DBS electrode to reduce common-mode noise, and served as inputs to a battery-powered preamplifier (A_1, SR560), which provided gain and high input impedance. Two additional amplifier stages (A_2 and A_3, SR560) were placed in series to increase gain further and to filter the signal with a 10 Hz to 10 kHz pass-band. Anti-parallel diode clamps (1N4154, Fairchild Semiconductor) were placed at the inputs of A_2 and A_3 to ground the line if the input voltage exceeded approximately ±0.7 V, thereby selectively clipping the stimulus artefact and enabling increased gain without saturation. To achieve further increases in gain, the signal paths in amplifiers A_2 and A_3 were internally grounded through an opto-isolated CMOS multiplexer (74HC4053), blanking the output for the duration of each stimulus pulse and the subsequent 100 μs. The rapid turn-off time of this CMOS switch (10 μs) ensured that short latency ECAP responses could still be recorded. In addition, a low-resistance, rapid-response PhotoMOS relay (AQV212(A), Panasonic) was used to disconnect the stimulating electrodes between DBS pulses. This limited capacitive discharge from the electrode-tissue interface through the stimulator after each pulse, and thereby reduced the duration of the stimulus artefact.[20] A 10 kΩ parallel resistor was placed across the stimulating electrodes to allow accumulated charge on the stimulating contacts to discharge between pulses. Further, this resistor enabled near-critical damping of the signal recovery from artefact to baseline. The digital pulse controlling the closing of the stimulator relay was turned off 40 μs before the end of the DBS pulse to account for the intrinsic delay of the relay. The digital pulses controlling the amplifier blanking and closing of the stimulator relay were turned on 2 ms before each DBS pulse to account for turn on delays, and to discharge any charge remaining on the stimulating electrodes.

Several strategies were implemented to reduce the risk of inadvertent electrical injury to the subject. The front end of each amplifier stage was AC-coupled to prevent exposure to DC voltages. Further, anti-series, current-limiting diodes (1N5285, Central Semiconductor) were placed between the DBS leads and each input to the preamplifier to limit current to less than 0.3 mA in the event of an instrumentation malfunction. Finally, DBS was applied through an optically-isolated stimulator (bp isolator, FHC) to keep the subject isolated from line power.

3.2. In Vitro Evaluation of the DBS-ECAP Instrumentation

In vitro experiments were conducted to characterize the capability of the DBS-ECAP instrumentation to reduce the stimulus artefact and record mock ECAPs (mECAPs) with high fidelity. Compared to a conventional amplifier setup (fig 3(ii)), the anti-parallel diodes in a three stage amplifier setup (fig 3(iii)) reduced the magnitude of the stimulus artefact (figure 4(a)) and enabled an increase in gain by a factor of 25 for all three contact configurations (table 1). Conversely, the amplifiers saturated at the equivalent gain without the use of the anti-parallel diodes (figure 4(b)). Even with the use of the diodes, there remained a relatively large amplitude, long duration stimulus artefact with a triphasic waveform shape (figure 4(c)), and the magnitude of this artefact increased when the contact configuration was changed from the monopolar symmetric configuration to either the monopolar asymmetric or bipolar configurations. The addition of the stimulator relay reduced the magnitude and duration of the third phase of the artefact by limiting capacitive discharge through the stimulator after each pulse. Subsequent addition of amplifier blanking suppressed the first two phases of the artefact (corresponding to the two phases of the DBS pulse). Compared to the conventional amplifier setup, use of the DBS-ECAP instrumentation with all components enabled an increase in gain by a factor of 1,000 to 5,000, depending on the contact configuration (table 1). However, the maximum gain used with the DBS-ECAP instrumentation during mECAP recording was limited to that of the diodes-only instrumentation (table 1) to avoid diode clipping of the mECAP and to enable comparison of these two recording system configurations at equal gain.

The recording fidelity of the DBS-ECAP instrumentation was examined through analysis of the distortion of mECAP signals generated by applying a single cycle of a sinusoidal current between two microelectrodes (figure 5). The higher gains enabled by the diodes-only instrumentation provided higher fidelity recording compared to the conventional amplifier setup. Further, the complete DBS-ECAP instrumentation limited the magnitude and duration of the third phase of the artefact, thereby reducing the temporal overlap of the artefact with short latency mECAPs and further increasing fidelity. Distortion decreased as DBS pulse width was reduced or mECAP latency increased (figure 6(a)). With 3 V DBS in the monopolar symmetric configuration, the DBS-ECAP instrumentation enabled high fidelity recording (DPS < 0.5) of small magnitude (0.18 $mV_{p\text{-}p}$) mECAPs at latencies of only 0.5 ms after DBS pulses of 50 or 100 μs duration, or latencies of 1 ms after long, asymmetric DBS pulses with 50 μs first phase and 500 μs second phase (figure 6(a), filled bars). In cases where a very short latency mECAP was coupled with a relatively long DBS pulse width, the mECAP was masked by amplifier blanking. Using the diodes-only instrumentation, the mECAP was more distorted (figure 6(a), open bars) and masked by the artefact in some trials, while using the conventional amplifier setup did not enable high fidelity recording of mECAPs for any combination of DBS pulse width and mECAP latency tested. Compared to the monopolar symmetric configuration, the minimum mECAP latencies required for high fidelity recording were generally equivalent for the bipolar configuration and longer for the monopolar asymmetric configuration with the DBS-ECAP instrumentation, and neither the diodes-only instrumentation nor the conventional amplifier could achieve high fidelity recording with these two contact configurations.

Distortion decreased as DBS amplitude was reduced or mECAP amplitude was increased (figure 6(b)). Short latency mECAPs overlapped with the stimulus artefact, and larger mECAP amplitudes or smaller DBS amplitudes increased the relative magnitude of the mECAP signal over the artefact. Applying 50 μs DBS pulses with the monopolar symmetric configuration, the DBS-ECAP instrumentation enabled high fidelity recordings of short latency (0.2 ms) mECAPs with amplitudes of only 0.18 $mV_{p\text{-}p}$ for 0 or 1 V DBS, and amplitudes of 0.53 $mV_{p\text{-}p}$ for 2 or 3 V DBS (figure 6(b), filled bars). With diodes-only instrumentation distortion was larger (figure 6(b), open bars), while the conventional amplifier setup could record mECAPs with high fidelity only at DBS amplitudes of 0 or 1 V, coupled with a large mECAP amplitude of 0.88 $mV_{p\text{-}p}$. Compared to the monopolar symmetric configuration, the mECAP amplitudes required for high fidelity recording were generally equivalent for the bipolar configuration and higher for the monopolar asymmetric configuration with the DBS-ECAP instrumentation. Further, high fidelity recording with these two contact configurations was feasible with the diodes-only system only in the absence of DBS, and was not possible with the conventional amplifier setup.

The disparity in minimum mECAP latencies and amplitudes required for high fidelity recording across contact configurations was generated by differences in the magnitude of the stimulus artefact, which increased from monopolar symmetric to asymmetric configurations, and from monopolar asymmetric to bipolar configurations (figure 4(c)), and in the magnitude of the recorded mECAP for a given input amplitude. For example, a mECAP with 0.1 $mA_{p\text{-}p}$ input amplitude corresponded to a recorded amplitude of 0.18, 0.11, and 0.30 $mV_{p\text{-}p}$ for the monopolar symmetric, monopolar asymmetric, and bipolar configurations, respectively. The relative magnitude of the stimulus artefact and mECAP has a critical influence on the recording fidelity (figure 6(b)), and likely led to the differences observed between contact configurations.

Use of the mini DBS electrode during *in vitro* testing generated similar stimulus artefact and mECAP waveforms to those recorded with the clinical DBS electrode (data not shown).

3.3. In Vivo ECAP Recording

The mini DBS electrode (figure 7(a)) was implanted in the ventrolateral (VL) nucleus of the cat thalamus for *in vivo* ECAP recording. The VL thalamus was identified with recordings of single thalamic neurons that exhibited increased activity during passive contralateral hind limb movement (figure 7(b)). Accurate implantation of the DBS electrode into the VL thalamus was confirmed subsequently by recording evoked responses from the DBS electrode during electrical stimulation of the contralateral sciatic nerve (figure 7(c)). Postmortem histology confirmed the position of the implanted electrode in the VL thalamus (figure 7(d)).

The *in vivo* ECAP response was recorded using the different recording system configurations to examine the relative performance of the DBS-ECAP instrumentation (figure 8). Comparing responses to cathodic- and anodic-phase first stimulation enables one to distinguish the physiological ECAP signal, which is similar for symmetric, biphasic pulses [46], from the stimulus artefact, which is inverted for opposite polarities. The stimulus artefact recorded with the conventional amplifier setup was reduced in magnitude with the use of the diodes-only instrumentation, enabling higher gains (figures 8(a),(b)), but the long duration of the artefact distorted the physiological ECAP. In contrast, the DBS-ECAP instrumentation suppressed the stimulus artefact and enabled high fidelity recording of ECAPs (figure 8(c)).

We examined how the ECAP characteristics were dependent on stimulation parameters (figure 9). In the monopolar symmetric configuration, ECAPs had an early positive (P1) phase followed by a later negative (N1) phase (figure 9(a)). The magnitude and duration of these phases generally increased with DBS pulse width and amplitude (figures 9(a),(b)), and the N1 phase was absent with low amplitude (1 V) DBS. Secondary positive (P2) and negative (N2) phases were observed at 10 Hz DBS (figure 9(a)). While these secondary phases were also present at the beginning of the stimulus train during 100 Hz DBS, their amplitudes progressively decayed during the stimulus train, and were not present in the average waveform. ECAPs recorded using the monopolar asymmetric configuration exhibited an early negative (N1') phase and later positive (P1') phase (figure 9(c)).

We measured the ECAP at multiple time points following euthanasia to confirm that the ECAP was a biological signal. While phases P1 and N1 were both still evident at 1 min following euthanasia (figure 10(a)), the latter was lost at 3 min (figure 10(b)). Postmortem recording at 5 min resulted only in a stimulus artefact, with inverted waveforms for opposite stimulation polarities, rather than a physiological ECAP response (figure 10(c)).

3.4 Computational Analysis of Stimulus Artefact Sources and Components for Artefact Reduction

An electrical circuit equivalent model was used to analyze the sources of the stimulus artefact recorded *in vitro* and *in vivo*, and to understand better the mechanism of artefact rejection by the stimulator relay of the DBS-ECAP instrumentation. The parameter values used in the circuit models are provided in table 2. The stimulus artefact was calculated as the differential voltage across the recording amplifier inputs, with and without use of the AQV212(A) stimulator relay, which had a 0.83 Ω on resistance and an operational timing matching that used experimentally.

The artefact calculated with the *in vitro* model (figure 11(a)) had a similar waveform shape to that recorded experimentally with the clinical DBS electrode in the saline bath using the conventional amplifier setup (figure 11(b)). The peak-to-peak magnitudes of the model and experimental artefacts were approximately 16 mV and 49 mV, respectively, and this difference likely resulted from errors associated with model assumptions. Use of the

stimulator relay in the *in vitro* experiment reduced, but did not eliminate, the third phase of the artefact observed with the conventional amplifier (figure 11(b)). Conversely, results from the circuit model indicated that turning the stimulator relay off immediately after the DBS pulse prevented capacitive discharging from the electrode-tissue interface and eliminated the third artefact phase (figure 11(a)). However, when a short (25 μs) turn off delay was added to the stimulator relay after the end of the DBS pulse, the model reproduced the reduced-magnitude third artefact phase seen experimentally. Although the digital pulse controlling the stimulator relay was turned off 40 μs before the end of the DBS pulse to account for this turn off delay in the *in vitro* experiment, the typical measured delay for the AQV212(A) relay is longer than 40 μs, and may have contributed to this observed post-stimulus delay time. The 25 μs turn off delay was used for subsequent model trials with the stimulator relay.

We next conducted sensitivity analysis to determine how the stimulus artefact calculated with the *in vivo* circuit model depended on the dielectric constant and tissue inhomogeneities. The stimulus artefact was calculated for dielectric constant values of neural tissue from 1×10^4 to 1×10^6 (figure 11(c)). The variations in tissue capacitance led to substantial changes in the waveform shape of the artefact, since higher capacitances resulted in longer time constants for charging and discharging of the tissue. Using a dielectric constant value of 3×10^5 resulted in an artefact (figure 11(d), black trace) that best matched the experimental waveform shape (figure 11(f)). We next investigated the effect of tissue inhomogeneity by decreasing the tissue resistance between contacts 0 and 1 by 5–10%, and increasing that between contacts 1 and 2 by the same percentage (figure 11(d)). A greater degree of inhomogeneity increased the magnitude of the stimulus artefact, due to the larger differential voltage generated at the two recording contacts. A change in tissue resistance values of 10% produced a model artefact waveform with a magnitude similar to that observed experimentally, and was used for subsequent artefact calculations. The presence of tissue inhomogeneities likely generated the larger stimulus artefact magnitudes *in vivo* compared to *in vitro*.

Discharging of the tissue capacitance following DBS pulses led to an increased duration of the third phase of the artefact *in vivo*. This phenomenon was observed experimentally (figure 11(f)), and was qualitatively reproduced with the circuit model (figure 11(e)). The stimulator relay did decrease capacitive discharging from the electrode-tissue interface and thereby reduce the magnitude of the third phase, but it did not prevent discharging of the tissue capacitance. The increase in artefact duration resulting from discharging of medium capacitance was only observed *in vivo*, since the permittivity of tissue is several orders of magnitude greater than that of saline.

The model was also used to investigate the increase in stimulus artefact amplitude in postmortem *in vivo* recordings (figure 10). Decreases in bulk tissue conductivity and permittivity, expected after euthanasia [44,45], increased the duration of the third artefact phase in the model (figure 11(g)). Further, local changes in brain conductivity that increased the extent of tissue inhomogeneity increased both the magnitude and duration of the artefact (figure 11(d)). These changes may explain the large amplitude artefacts observed 5 minutes after euthanasia.

4. Discussion

We designed and evaluated the performance of instrumentation for high fidelity recording of ECAPs from the DBS electrode during stimulation. By reducing the magnitude and duration of the stimulus artefact, the DBS-ECAP instrumentation enabled recording of small amplitude, short latency mECAPs *in vitro*. The ability of the instrumentation to record

physiological ECAPs was confirmed during *in vivo* DBS in the cat thalamus. The characteristics of the *in vivo* ECAP were dependent on stimulation parameters and may provide insight into the type and spatial extent of neural element activation during stimulation. Thus, the ECAP signal may be a suitable feedback control signal for tuning DBS parameters and in closed-loop DBS systems.

4.1 Design and Evaluation of Instrumentation

Several hardware-based strategies were used to limit the stimulus artefact. We employed multiple amplifier stages with anti-parallel diode clamps at the inputs to clip selectively the stimulus artefact and provide overvoltage protection. The magnitude of the artefact was reduced further by amplifier blanking, in which the signal paths in the second and third amplifier stages were grounded during each DBS pulse. To reduce the duration of the third phase of the artefact, and minimize the extent of temporal overlap with the ECAP, we used a stimulator relay to reduce capacitive discharge of the electrode-tissue interface immediately after each DBS pulse.[20] This relay disconnected the low impedance path available through the constant-voltage stimulator, thereby limiting the discharging current through the high impedance 10 kW parallel resistance. Accumulated charge was able to discharge between pulses through this parallel resistance and during the 2 ms pre-stimulus period in which the relay was closed. The parallel resistance also enabled near-critical damping of the signal recovery from artefact to baseline. Replacing the resistor with a potentiometer could enable rapid selection of a parallel resistance that achieved full critical damping of the system.

Other techniques used to suppress the stimulus artefact in neural recordings were not optimal for this application. Signal processing techniques such as curve fitting, template subtraction, polarity averaging, and masker-probe paradigms are applied after the signal has been amplified and require lower gains to avoid saturation. Further, the performance of the template subtraction and polarity averaging techniques suffers from the assumptions that the artefact shape is constant between stimulus pulses [21] and that the artefact perfectly follows the stimulus pulse in polarity [47], respectively. Signal filtering was not feasible due to overlapping frequency spectra of the ECAP signal and stimulus artefact. Alternatively, sample-and-hold amplifiers have not demonstrated the capacity to make artefact-free recordings of sub-ms latency neural activity, as required to capture physiological ECAPs, and have yielded inconsistent results.

Our novel DBS-ECAP instrumentation reduced the artefact magnitude and enabled a total *in vitro* gain of 40,000 to 100,000 without saturation during 3 V DBS, depending on the contact configuration. These gains far surpassed the conventional amplifier setup by a factor of 1,000 to 5,000. Further, the reductions in artefact duration and use of high gains facilitated high fidelity recording of physiologically-realistic mECAPs, at latencies as short as 0.5 ms and amplitudes as small as 0.11 to 0.30 $mV_{P\text{-}P}$. This was the case for all contact configurations when using clinically-relevant DBS parameters of 3 V amplitude, 100 Hz frequency, 50 μs pulse width, and was not feasible with a conventional amplifier setup. Long, asymmetric DBS pulses precluded high fidelity recording of ECAPs with the DBS-ECAP instrumentation except at latencies of at least 1 ms. Since physiological ECAPs have latencies in the sub-ms range, it may not be feasible to use long, asymmetric pulses, such as those generated by the present clinical device [48], during ECAP recording.

The contact configurations used for stimulation and ECAP recording influenced the fidelity of the recording. The stimulus artefact magnitude was larger when the voltages generated during stimulation were not symmetrical at the recording contacts (i.e., the monopolar asymmetric and bipolar configurations). This required reductions in amplifier gain (table 1) and made it more challenging to record short latency mECAPs. Moreover, the recorded mECAP magnitude increased with the distance between recording contacts (maximal in the

bipolar configuration), since the contacts measured a larger differential-mode signal. Collectively, this suggests that high fidelity recording is most challenging in the monopolar asymmetric configuration, due to the short distance between recording contacts and their non-symmetrical positioning about the stimulating contact. This was confirmed through the distortion analysis of mECAP recordings made *in vitro* across contact configurations.

The artefact waveforms calculated with the electrical circuit equivalent model were similar in magnitude and shape to the *in vitro* and *in vivo* artefacts, and provided insight into the origin of the artefact (figure 11). In the *in vitro* experiment, the only source of the third artefact phase was capacitive discharging from the electrode-tissue interface, which was limited with the use of the stimulator relay. However, the turn off delay of the relay, which was approximately 25 μs after the end of the DBS pulse, allowed some discharging. Consequently, the size of the third phase was reduced but not eliminated. This suggests that using a stimulator relay with a shorter turn off delay may improve the performance of this system. The model indicated that there were two sources of the third artefact phase observed *in vivo*: capacitive discharging after each DBS pulse of (1) the tissue capacitance, and (2) the electrode-tissue interface. Previous computational [39,49] and experimental [50] studies have also demonstrated that the tissue capacitance is charged during the DBS pulse (influencing the DBS waveform shape). The stimulator relay cannot suppress the artefact resulting from discharging of the tissue capacitance, and thus the third phase is larger *in vivo* than *in vitro*. We investigated a means to rapidly discharge the tissue capacitance by shorting the amplifier inputs with a PhotoMOS relay for 100 μs immediately after each pulse. However, this technique did not reduce the third phase of the *in vivo* artefact, and electrical equivalent circuit modeling indicated that the lack of effect was caused by negligible current flow through the relay due to its internal impedance (data not shown). Finally, the peak-to-peak magnitude of the artefact recorded with the conventional amplifier was greater *in vivo* than *in vitro*, and results from the circuit model suggest that this may have been caused by inhomogeneities in the neural tissue, which were not present in the saline bath.

4.2 Insight Provided by the Physiological ECAP

The results from our *in vivo* experiment confirmed that physiological ECAPs could be recorded during thalamic DBS. The VL thalamus is the feline homologue of the Vim thalamus in primates, functioning as a relay from muscle afferents to cortex area 3A.[33] We used several techniques to identify the VL thalamus and accurately implant the DBS electrode into this nucleus. The DBS-ECAP instrumentation enabled high gain recordings of ECAPs, uncontaminated by the stimulus artefact, during DBS of the VL thalamus. This could be performed using both the monopolar symmetric and asymmetric configurations (figure 9), of which the latter was revealed by *in vitro* analysis to be the most challenging configuration for high fidelity recording. The similarity of ECAP waveform shapes recorded during cathodic- and anodic-phase first polarity stimulation corroborated the neural origin of the signal, and the elimination of the ECAP response at 5 min after euthanasia (figure 10) further verified the biological origin of the recorded signal. The increase in stimulus artefact magnitude observed after euthanasia could have been caused by decreases in bulk tissue conductivity and permittivity [44,45] and/or local changes in brain conductivity that increased the extent of tissue inhomogeneity. Electrical circuit equivalent modeling indicated that these changes increased the magnitude and duration of the third phase, which would be recorded experimentally by the DBS-ECAP instrumentation.

Measuring the ECAP across DBS parameters provided insight into the activation patterns during DBS. The magnitude and duration of the ECAP phases generally increased with DBS amplitude and pulse width, as a result of activation of additional neural elements having higher stimulation thresholds.[51] ECAPs generated with the monopolar symmetric

configuration had an early positive (P1) phase and later (N1) negative phase. To interpret this finding, we used results from the modeled cochlear ECAP response, in which a large negative phase, flanked on each side by small positive phases, corresponded to action potential propagation near the recording contact.[52] We propose that P1 was generated by early dorsal activity (near the negative recording contact) whereas N1 corresponded to later ventral activity (near the positive contact). Furthermore, we observed secondary positive (P2) and negative (N2) phases during low frequency DBS, and at the beginning of the pulse train during high frequency DBS. This suggests that the P2 and N2 phases corresponded to post-synaptic activity, and the loss of these phases at high stimulation frequencies corresponded to a reduction in post-synaptic activity.[53] Recording the ECAP with the monopolar asymmetric configuration revealed an early negative (N1') phase and later positive (P1') phase. These two phases likely corresponded to dorsal-to-ventral propagation of action potentials, initiated in projecting cells near the stimulating contact, and projecting first past the positive recording contact (N1') and subsequently past the negative contact (P1').

4.3 Study Limitations

The electrical circuit equivalent model provided insight into the sources of the stimulus artefact; however, there are several limitations that should be noted. First, calculations of medium resistance and capacitance assumed a spherical volume conductor encapsulating the DBS electrode, with the return electrode at the volume conductor boundary. Further, the medium capacitance calculations assumed that the DBS contacts were spherical. In the *in vitro* and *in vivo* experiments, the return electrode did not bound the DBS electrode, but rather was located at a single, distant position (figure 1). This model assumption may have resulted in underestimation of the medium resistance and overestimation of the medium capacitance between DBS contacts and the return electrode. Further, neither the saline tank nor the DBS contacts were actually spherical, but these assumptions likely had a negligible effect on model results due to the large difference in size between DBS contacts and the volume conductor, which would be expected to mitigate the effects of these geometric approximations.

The second limitation was an assumption in the circuit model that the mini DBS electrode had the same electrode-tissue interface properties as the clinical DBS electrode, for which the impedance values were measured.[35] However, when the interface resistance and capacitance values of the mini DBS electrode were modified to account for the smaller surface area, the effect on the artefact waveform was negligible (data not shown). Third, this model did not include capacitive coupling between stimulating and recording leads [20,54], which was reasonable considering this would generate a common-mode stimulus artefact and be rejected at the differential preamplifier stage. The fourth limitation was that we did not account for the frequency-dependence of tissue permittivity [55] in calculating bulk volume capacitance, and it remains unclear which permittivity value best represents brain tissue.[39] However, under conditions of voltage-controlled stimulation in a homogenous medium, using a frequency-dependent permittivity can closely approximate the solution of a fully dispersive model.[56] Fifth, the medium capacitance between two DBS contacts was not included in the circuit model.

The final major limitation of the circuit model was that changes in neural tissue properties measured after euthanasia in literature were made in porcine [44] and bovine [45] brains, rather than the cat. Further, the change in permittivity was measured at high frequencies (900 MHz), outside of the bandwidth of the DBS pulse.[44] Similarly, the change in conductivity was measured at a relatively high frequency (100 kHz).[45] Therefore the neural tissue property values used in the postmortem *in vivo* circuit model were only approximations for impedance changes in the cat brain during DBS.

A limitation of the experimental methods used in this study was that a clinical DBS electrode was used for most of the *in vitro* testing, whereas a mini DBS electrode was used in the *in vivo* experiments. We chose to evaluate the *in vitro* performance of the DBS-ECAP instrumentation with the clinical DBS electrode since the ECAP recording technique is intended for clinical translation. Conversely, the mini DBS electrode was more appropriate for the size of the cat brain. Nevertheless, the stimulus artefact and mECAP waveforms recorded with the clinical DBS electrode were very similar to those recorded with the mini DBS electrode during *in vitro* testing, suggesting a small effect of DBS geometry on ECAP recordings.

Conclusions

We developed novel instrumentation and demonstrated high fidelity recordings of mECAPs *in vitro* and physiological ECAPs *in vivo* during DBS. The *in vivo* ECAP provided information about the spatiotemporal activation pattern (timing and polarity of ECAP phases), the spatial extent of this activation (ECAP magnitude), and the types of elements activated (i.e., post-synaptic cells). The presence of these signatures suggests that the ECAP could provide a suitable feedback control signal for the selection of stimulation parameters during clinical programming sessions, or in closed-loop DBS systems that automatically adjust stimulation parameters as the disease progresses or the response to DBS changes over time.[57]

Acknowledgments

The authors would like to thank Gilda Mills for animal care and surgical assistance and Thomas Jochum for reviewing the manuscript. This work was supported by NIH F31-NS-070460 and the Duke University Department of Biomedical Engineering Robert Plonsey Fellowship.

References

[1]. Benabid AL, Pollak P, Gervason C, Hoffmann D, Gao DM, Hommel M, Perret JE, de Rougemont J. Long-term suppression of tremor by chronic stimulation of the ventral intermediate thalamic nucleus. Lancet. 1991; 337:403–6. [PubMed: 1671433]

[2]. Pahwa R, et al. Long-term evaluation of deep brain stimulation of the thalamus. J Neurosurg. 2006; 104:506–12. [PubMed: 16619653]

[3]. Benabid AL, Pollak P, Gross C, Hoffmann D, Benazzouz A, Gao DM, Laurent A, Gentil M, Perret J. Acute and long-term effects of subthalamic nucleus stimulation in Parkinson's disease. Stereotact Funct Neurosurg. 1994; 62:76–84. [PubMed: 7631092]

[4]. Hodaie M, Wennberg RA, Dostrovsky JO, Lozano AM. Chronic anterior thalamus stimulation for intractable epilepsy. Epilepsia. 2002; 43:603–8. [PubMed: 12060019]

[5]. Kuncel AM, Grill WM. Selection of stimulus parameters for deep brain stimulation. Clin Neurophysiol. 2004; 115:2431–41. [PubMed: 15465430]

[6]. Temperli P, Ghika J, Villemure JG, Burkhard PR, Bogousslavsky J, Vingerhoets FJ. How do parkinsonian signs return after discontinuation of subthalamic DBS? Neurology. 2003; 60:78–81. [PubMed: 12525722]

[7]. Beuter A, Titcombe MS. Modulation of tremor amplitude during deep brain stimulation at different frequencies. Brain Cogn. 2003; 53:190–2. [PubMed: 14607145]

[8]. Ondo WG, Bronte-Stewart H. The North American survey of placement and adjustment strategies for deep brain stimulation. Stereotact Funct Neurosurg. 2005; 83:142–7. [PubMed: 16205106]

[9]. Okun MS, Tagliati M, Pourfar M, Fernandez HH, Rodriguez RL, Alterman RL, Foote KD. Management of referred deep brain stimulation failures: a retrospective analysis from 2 movement disorders centers. Arch Neurol. 2005; 62:1250–5. [PubMed: 15956104]

[10]. Moro E, Poon YY, Lozano AM, Saint-Cyr JA, Lang AE. Subthalamic nucleus stimulation: improvements in outcome with reprogramming. Arch Neurol. 2006; 63:1266–72. [PubMed: 16831958]

[11]. Marceglia S, Rossi L, Foffani G, Bianchi A, Cerutti S, Priori A. Basal ganglia local field potentials: applications in the development of new deep brain stimulation devices for movement disorders. Expert Rev Med Devices. 2007; 4:605–14. [PubMed: 17850195]

[12]. Kane A, Hutchison WD, Hodaie M, Lozano AM, Dostrovsky JO. Enhanced synchronization of thalamic theta band local field potentials in patients with essential tremor. Exp Neurol. 2009; 217:171–6. [PubMed: 19233174]

[13]. Brown P, Williams D. Basal ganglia local field potential activity: character and functional significance in the human. Clin Neurophysiol. 2005; 116:2510–9. [PubMed: 16029963]

[14]. Rossi L, Marceglia S, Foffani G, Cogiamanian F, Tamma F, Rampini P, Barbieri S, Bracchi F, Priori A. Subthalamic local field potential oscillations during ongoing deep brain stimulation in Parkinson's disease. Brain Res Bull. 2008; 76:512–21. [PubMed: 18534260]

[15]. Bronte-Stewart H, Barberini C, Koop MM, Hill BC, Henderson JM, Wingeier B. The STN beta-band profile in Parkinson's disease is stationary and shows prolonged attenuation after deep brain stimulation. Exp Neurol. 2009; 215:20–8. [PubMed: 18929561]

[16]. Kuncel AM, Cooper SE, Wolgamuth BR, Grill WM. Amplitude- and frequency-dependent changes in neuronal regularity parallel changes in tremor with thalamic deep brain stimulation. IEEE Trans Neural Syst Rehabil Eng. 2007; 15:190–7. [PubMed: 17601188]

[17]. Miller CA, Brown CJ, Abbas PJ, Chi SL. The clinical application of potentials evoked from the peripheral auditory system. Hear Res. 2008; 242:184–97. [PubMed: 18515023]

[18]. Jeon EK, Brown CJ, Etler CP, O'Brien S, Chiou LK, Abbas PJ. Comparison of electrically evoked compound action potential thresholds and loudness estimates for the stimuli used to program the Advanced Bionics cochlear implant. J Am Acad Audiol. 2010; 21:16–27. [PubMed: 20085196]

[19]. Rossi L, Foffani G, Marceglia S, Bracchi F, Barbieri S, Priori A. An electronic device for artefact suppression in human local field potential recordings during deep brain stimulation. J Neural Eng. 2007; 4:96–106. [PubMed: 17409484]

[20]. McGill KC, Cummins KL, Dorfman LJ, Berlizot BB, Leutkemeyer K, Nishimura DG, Widrow B. On the nature and elimination of stimulus artifact in nerve signals evoked and recorded using surface electrodes. IEEE Trans Biomed Eng. 1982; 29:129–37. [PubMed: 7056556]

[21]. Wagenaar DA, Potter SM. Real-time multi-channel stimulus artifact suppression by local curve fitting. J Neurosci Methods. 2002; 120:113–20. [PubMed: 12385761]

[22]. Hashimoto T, Elder CM, Vitek JL. A template subtraction method for stimulus artifact removal in high-frequency deep brain stimulation. J Neurosci Methods. 2002; 113:181–6. [PubMed: 11772439]

[23]. Brown CJ, Abbas PJ. Electrically evoked whole-nerve action potentials: parametric data from the cat. J Acoust Soc Am. 1990; 88:2205–10. [PubMed: 2269736]

[24]. Miller CA, Abbas PJ, Brown CJ. An improved method of reducing stimulus artifact in the electrically evoked whole-nerve potential. Ear Hear. 2000; 21:280–90. [PubMed: 10981604]

[25]. Miller CA, Abbas PJ, Robinson BK, Rubinstein JT, Matsuoka AJ. Electrically evoked single-fiber action potentials from cat: responses to monopolar, monophasic stimulation. Hear Res. 1999; 130:197–218. [PubMed: 10320109]

[26]. Alvarez I, de la Torre A, Sainz M, Roldan C, Schoesser H, Spitzer P. Generalized alternating stimulation: a novel method to reduce stimulus artifact in electrically evoked compound action potentials. J Neurosci Methods. 2007; 165:95–103. [PubMed: 17624444]

[27]. Babb TL, Mariani E, Strain GM, Lieb JP, Soper HV, Crandall PH. A sample and hold amplifier system for stimulus artifact suppression. Electroencephalogr Clin Neurophysiol. 1978; 44:528–31. [PubMed: 76562]

[28]. Blum RA, Ross JD, Brown EA, DeWeerth SP. An integrated system for simultaneous, multichannel neuronal stimulation and recording. IEEE Trans Circ Syst. 2007; 54:2608–2618.

[29]. Jimbo Y, Kasai N, Torimitsu K, Tateno T, Robinson HP. A system for MEA-based multisite stimulation. IEEE Trans Biomed Eng. 2003; 50:241–8. [PubMed: 12665038]

[30]. Grumet AE, Wyatt JL Jr. Rizzo JF 3rd. Multi-electrode stimulation and recording in the isolated retina. J Neurosci Methods. 2000; 101:31–42. [PubMed: 10967359]

[31]. Kent AR, Grill WM. Instrumentation to record evoked potentials for closed-loop control of deep brain stimulation. Conf Proc IEEE Eng Med Biol Soc. 2011:6777–80. [PubMed: 22255894]

[32]. Snider, RS.; Niemer, WT. A Stereotaxic Atlas of the Cat Brain. The University of Chicago Press; Chicago: 1961.

[33]. Berman, AL.; Jones, EG. The Thalamus and Basal Telencephalon of the Cat. The University of Wisconsin Press; Madison: 1982.

[34]. McConnell GC, Rees HD, Levey AI, Gutekunst CA, Gross RE, Bellamkonda RV. Implanted neural electrodes cause chronic, local inflammation that is correlated with local neurodegeneration. J Neural Eng. 2009; 6:056003. [PubMed: 19700815]

[35]. Wei XF, Grill WM. Impedance characteristics of deep brain stimulation electrodes in vitro and in vivo. J Neural Eng. 2009; 6:046008. [PubMed: 19587394]

[36]. Geddes LA, Baker LE. The specific resistance of biological material--a compendium of data for the biomedical engineer and physiologist. Med Biol Eng. 1967; 5:271–93. [PubMed: 6068939]

[37]. Ranck JB Jr. Specific impedance of rabbit cerebral cortex. Exp Neurol. 1963; 7:144–52. [PubMed: 13990734]

[38]. Yousif N, Bayford R, Liu X. The influence of reactivity of the electrode-brain interface on the crossing electric current in therapeutic deep brain stimulation. Neuroscience. 2008; 156:597–606. [PubMed: 18761058]

[39]. Butson CR, McIntyre CC. Tissue and electrode capacitance reduce neural activation volumes during deep brain stimulation. Clin Neurophysiol. 2005; 116:2490–500. [PubMed: 16125463]

[40]. Wang P, Anderko A. Computation of dielectric constants of solvent mixtures and electrolyte solutions. Fluid Phase Equilib. 2001; 186:103–22.

[41]. Foster KR, Schwan HP. Dielectric properties of tissues and biological materials: a critical review. Crit Rev Biomed Eng. 1989; 17:25–104. [PubMed: 2651001]

[42]. Schwan HP, Kay CF. The conductivity of living tissues. Ann N Y Acad Sci. 1957; 65:1007–13. [PubMed: 13459187]

[43]. Young, HD.; Freedman, RA. University Physics. Pearson Education; San Francisco: 2004.

[44]. Schmid G, Neubauer G, Illievich UM, Alesch F. Dielectric properties of porcine brain tissue in the transition from life to death at frequencies from 800 to 1900 MHz. Bioelectromagnetics. 2003; 24:413–22. [PubMed: 12929160]

[45]. Surowiec A, Stuchly SS, Swarup A. Postmortem changes of the dielectric properties of bovine brain tissues at low radiofrequencies. Bioelectromagnetics. 1986; 7:31–43. [PubMed: 3730000]

[46]. McIntyre CC, Grill WM. Selective microstimulation of central nervous system neurons. Ann Biomed Eng. 2000; 28:219–33. [PubMed: 10784087]

[47]. Bahmer A, Peter O, Baumann U. Recording and analysis of electrically evoked compound action potentials (ECAPs) with MED-EL cochlear implants and different artifact reduction strategies in Matlab. J Neurosci Methods. 2010; 191:66–74. [PubMed: 20558202]

[48]. Miocinovic S, Lempka SF, Russo GS, Maks CB, Butson CR, Sakaie KE, Vitek JL, McIntyre CC. Experimental and theoretical characterization of the voltage distribution generated by deep brain stimulation. Exp Neurol. 2009; 216:166–76. [PubMed: 19118551]

[49]. Tracey B, Williams M. Computationally efficient bioelectric field modeling and effects of frequency-dependent tissue capacitance. J Neural Eng. 2011; 8:036017. [PubMed: 21540485]

[50]. Lempka SF, Johnson MD, Miocinovic S, Vitek JL, McIntyre CC. Current-controlled deep brain stimulation reduces in vivo voltage fluctuations observed during voltage-controlled stimulation. Clin Neurophysiol. 2010; 121:2128–33. [PubMed: 20493764]

[51]. Ranck JB Jr. Which elements are excited in electrical stimulation of mammalian central nervous system: a review. Brain Res. 1975; 98:417–40. [PubMed: 1102064]

[52]. Briaire JJ, Frijns JH. Unraveling the electrically evoked compound action potential. Hear Res. 2005; 205:143–56. [PubMed: 15953524]

[53]. Anderson TR, Hu B, Iremonger K, Kiss ZH. Selective attenuation of afferent synaptic transmission as a mechanism of thalamic deep brain stimulation-induced tremor arrest. J Neurosci. 2006; 26:841–50. [PubMed: 16421304]

[54]. Grumet, AE. PhD thesis. Massachusetts Institute of Technology; 1999. Electric stimulation parameters for an epi-retinal prosthesis.

[55]. Bossetti CA, Birdno MJ, Grill WM. Analysis of the quasi-static approximation for calculating potentials generated by neural stimulation. J Neural Eng. 2008; 5:44–53. [PubMed: 18310810]

[56]. Grant PF, Lowery MM. Effect of dispersive conductivity and permittivity in volume conductor models of deep brain stimulation. IEEE Trans Biomed Eng. 2010; 57:2386–93. [PubMed: 20595081]

[57]. Santaniello S, Fiengo G, Glielmo L, Grill WM. Closed-loop control of deep brain stimulation: a simulation study. IEEE Trans Neural Syst Rehabil Eng. 2011; 19:15–24. [PubMed: 20889437]

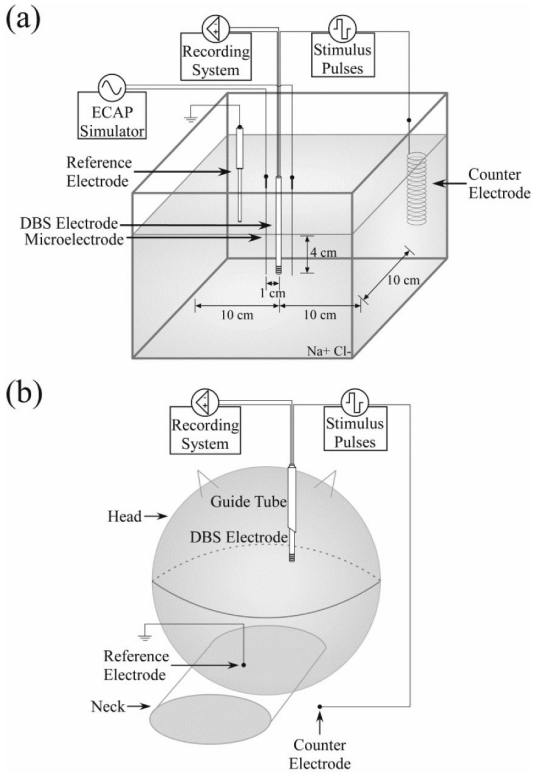

Figure 1.

Schematic of the experimental setups used to record evoked compound action potentials (ECAPs) during deep brain stimulation (DBS). (a) For *in vitro* testing, the DBS electrode, tungsten microelectrodes, Ag/AgCl recording circuit reference electrode, and counter electrode were immersed in a saline bath. The microelectrodes were positioned on either side of the DBS electrode to deliver the mock ECAP. (b) For *in vivo* testing, the mini DBS electrode was implanted through a guide tube into the ventrolateral nucleus of the thalamus in an anesthetized cat. We used a stainless steel retractor placed in the ipsilateral chest muscle as the counter electrode, and a Ag/AgCl electrode placed on the back of the neck as the recording circuit reference.

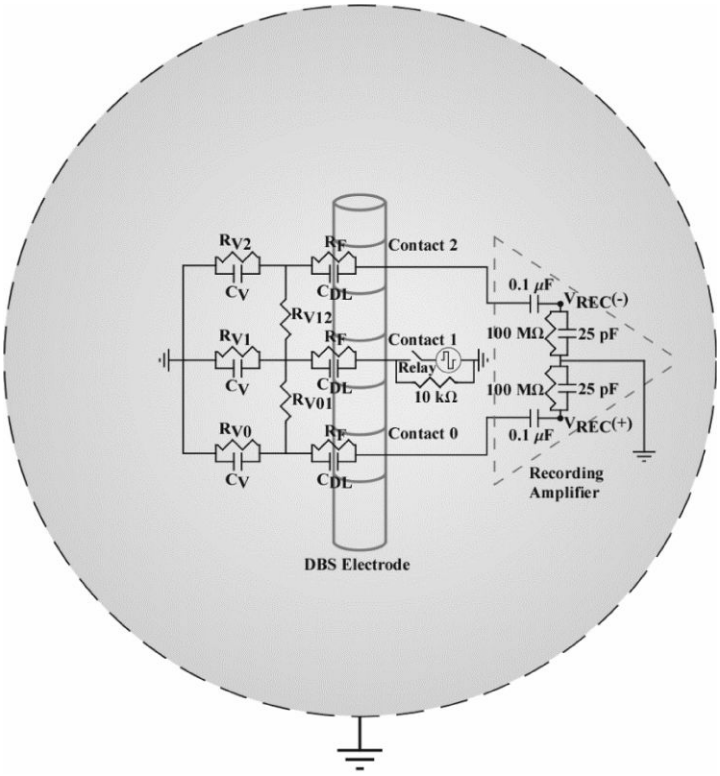

Figure 2.

Electrical circuit equivalent model used to calculate the stimulus artefact generated by DBS applied between contact 1 and a spherical return electrode, with differential recordings made from contacts 0 and 2 (monopolar symmetric configuration). The electrode-tissue interface was composed of a parallel double-layer capacitance (C_{DL}) and charge transfer Faradaic resistance (R_F). The volume conductor included both the resistance between contacts (R_{V01} and R_{V12}) and the resistance between each contact and the return electrode (R_{V0}, R_{V1}, and R_{V2}). The capacitance of the volume conductor (C_V) was parallel to the resistance between contacts and the return electrode. The input impedance of the recording amplifier was represented in the model, and the model output was the recorded differential voltage (V_{REC}) across the amplifier impedance.

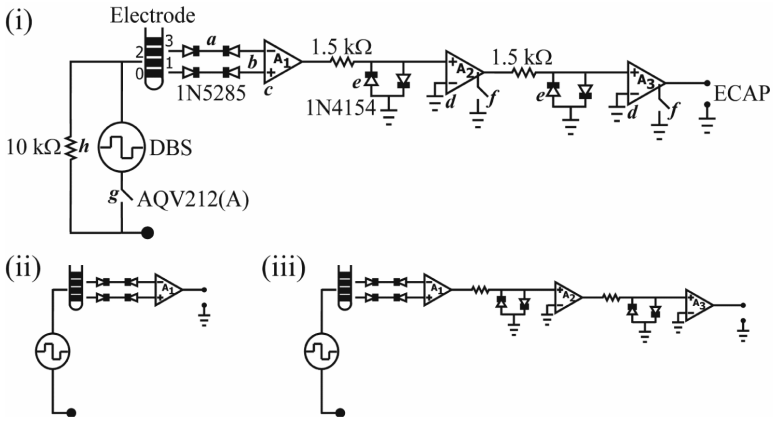

Figure 3.

(i) Diagram of the DBS-ECAP instrumentation used for stimulus artefact reduction and ECAP recording during DBS. (a) Anti-series, current-limiting diodes (1N5285) were connected to the DBS lead prior to the amplification stages. (b) Differential recordings were made from two DBS contacts, and (c) served as inputs to the preamplifier (A_1). (d) Two additional series amplifier stages (A_2 and A_3) further increased the gain and filtered the signal with a 10 Hz to 10 kHz pass-band. (e) Anti-parallel diodes (1N4154) were placed at the inputs of A_2 and A_3. (f) During each stimulus pulse, an opto-isolated CMOS multiplexer (74HC4053) internally grounded the signal path in amplifiers A_2 and A_3. (g) A PhotoMOS relay (AQV212(A)) disconnected the stimulating electrodes in between DBS pulses. (h) The parallel resistance enabled any accumulated charge on the stimulating electrodes to discharge between pulses, and enabled near-critical damping of the signal recovery from artefact to baseline. Diagrams of the (ii) conventional amplifier setup, and (iii) diodes-only instrumentation are also provided.

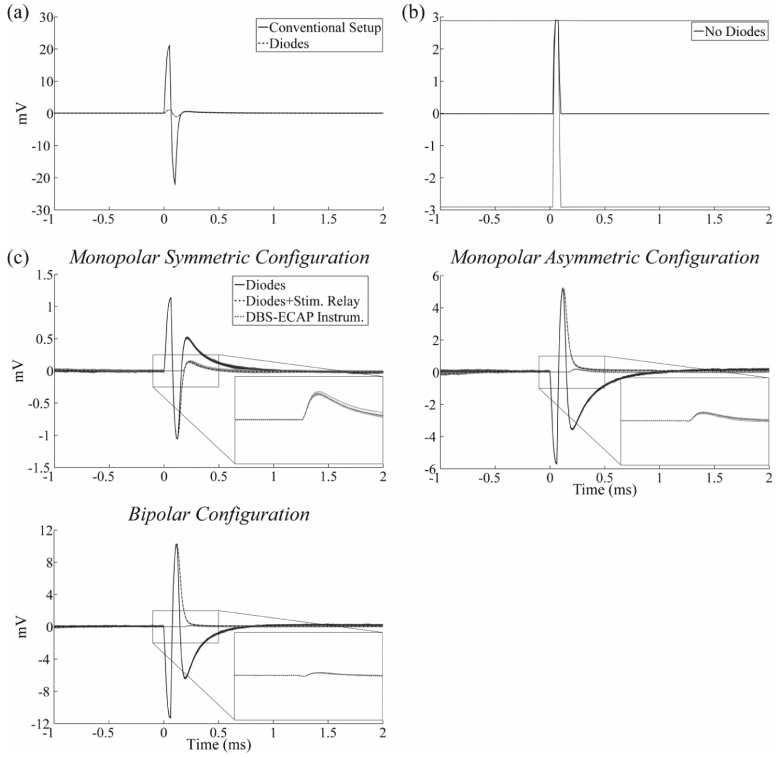

Figure 4.

In vitro stimulus artefact waveforms measured with the different recording system configurations. DBS was applied at time 0 with 3 V amplitude, 100 Hz frequency, 50 μs pulse width, and cathodic-phase first polarity. Unless otherwise specified, the monopolar symmetric configuration was used for these data. The stimulus-triggered average waveform (black traces) and single trials (gray traces) are shown. The magnitudes of the recorded waveforms were gain-corrected. (a) Comparison of artefacts recorded with a conventional amplifier setup (solid trace) and with the diodes-only instrumentation (dashed trace). (b) Using the series amplifier setup without anti-parallel diodes caused amplifier saturation at the equivalent gain. (c) Comparison of artefacts recorded across contact configurations with the diodes-only instrumentation (solid trace), after the addition of the stimulator relay (dashed trace), and with the DBS-ECAP instrumentation (dotted trace) with all circuit components present. The insets show a zoomed view of the stimulus artefact waveforms for the DBS-ECAP instrumentation.

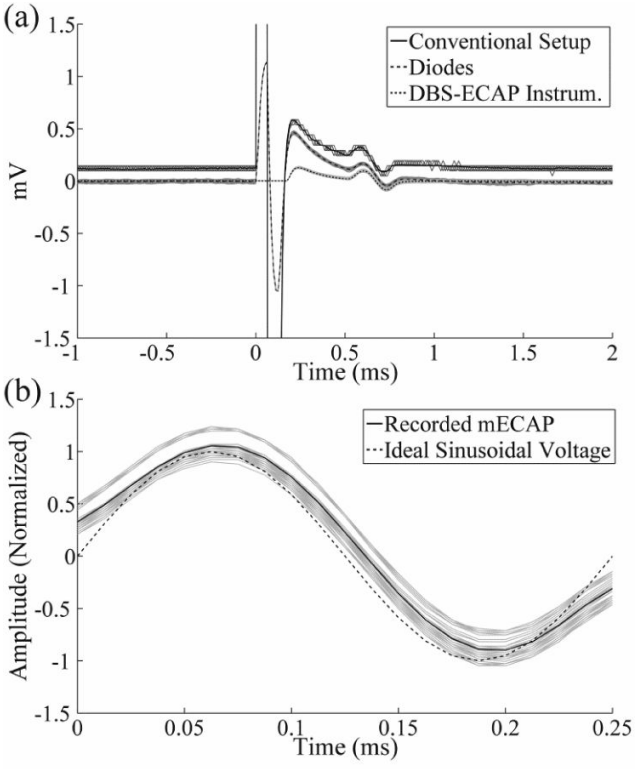

Figure 5.

(a) *In vitro* stimulus artefact and mock ECAP (mECAP) waveforms measured with the different recording system configurations using the monopolar symmetric configuration. DBS was applied at time 0 with 3 V amplitude, 100 Hz frequency, 50 μs pulse width, and cathodic-phase first polarity. Each DBS pulse triggered a 4 kHz sinusoidal mECAP with 0.18 $mV_{p\text{-}p}$ amplitude (0.1 $mA_{p\text{-}p}$ input amplitude) and 0.5 ms latency. The waveforms are compared for the conventional amplifier setup (solid trace), diodes-only instrumentation (dashed trace), and DBS-ECAP instrumentation (dotted trace). The stimulus-triggered average waveform (black traces) and single trials (gray traces) are shown. The magnitudes of the recorded waveforms were gain-corrected. (b) Comparison of the mECAP recorded with the DBS-ECAP instrumentation (solid trace) and an ideal mECAP sinusoid (dashed trace). For the recorded signal, the stimulus-triggered average waveform (black trace) and single trials (gray traces) are shown. The magnitudes of the recorded and ideal sinusoids are normalized to that of the ideal sinusoid. The distortion per sample value of this recorded mECAP is 0.17.

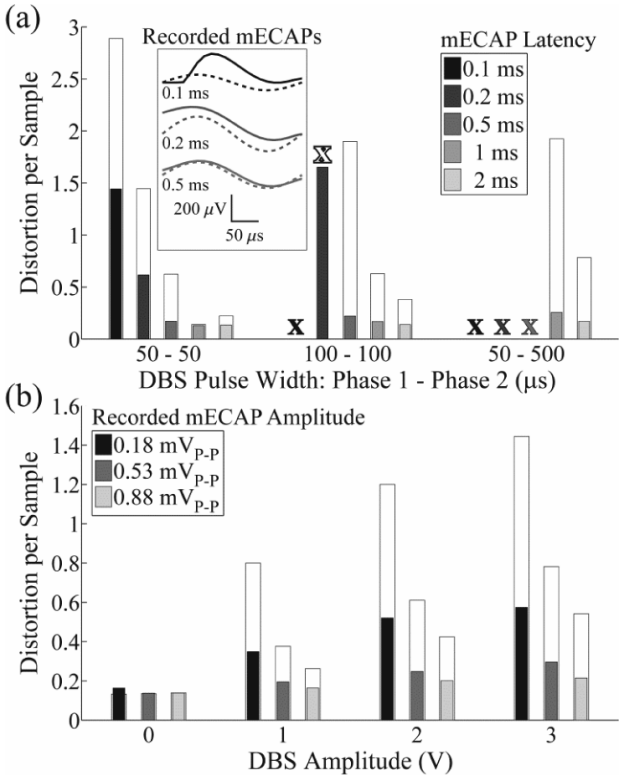

Figure 6.

Distortion per sample of the mECAP across DBS and mECAP stimulation parameters, measured *in vitro* with the monopolar symmetric configuration. (a) Effect of DBS pulse width and mECAP latency on distortion. DBS parameters were 3 V amplitude, 100 Hz frequency, and cathodic-phase first polarity, and sinusoidal mECAP parameters were 0.18 $mV_{P\text{-}P}$ amplitude (0.1 $mA_{P\text{-}P}$ input amplitude) and 4 kHz frequency. The narrow, filled bars show distortion values for the DBS-ECAP instrumentation, whereas the wider, open bars show the distortion when the diodes-only instrumentation was used. For some trials, the mECAP was masked and these are marked by a white X when masked with diodes-only instrumentation, and a filled X when masked with both diodes-only and DBS-ECAP instrumentation systems. The inset shows mECAPs recorded with the DBS-ECAP instrumentation (solid trace) and ideal mECAP sinusoid (dashed trace) for a DBS pulse width of 50 μs and the denoted mECAP latency. (b) Effect of DBS and mECAP amplitudes on distortion. DBS parameters were 50 μs pulse width, 100 Hz frequency, and cathodic-phase first polarity, and the sinusoidal mECAP parameters were 0.2 ms latency and 4 kHz frequency. Data presentation is otherwise identical to that in (a).

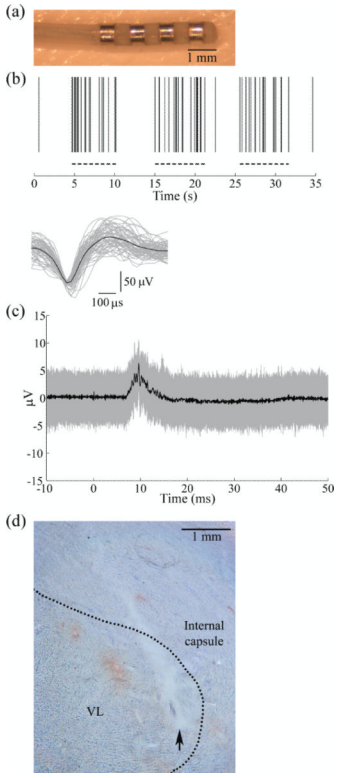

Figure 7.

The ventrolateral (VL) nucleus of the thalamus was targeted for DBS electrode implantation in an anesthetized cat. (a) A mini DBS electrode was used for *in vivo* ECAP recording during thalamic DBS. (b) The location of the VL thalamus was identified by recording the activity of single thalamic neurons with a microelectrode during stereotactic surgery. *Top*: Raster plot of spiking in a neuron showing increased activity during passive contralateral hind limb movement (dashed lines). *Bottom*: Waveforms of 61 discriminated spike waveforms recorded from the neuron (gray traces) and average waveform across all spikes (black trace). (c) Accurate implantation into the VL thalamus was verified by recording the evoked response from the DBS electrode during contralateral sciatic nerve stimulation, applied at time 0. The stimulus-triggered average (black trace) and single trials (gray traces) are shown. (d) Postmortem histology confirmed the location of the DBS electrode location within the VL thalamus, with the nuclear boundary indicated by the dashed line. The arrow indicates the location of the ventral tip of the electrode.

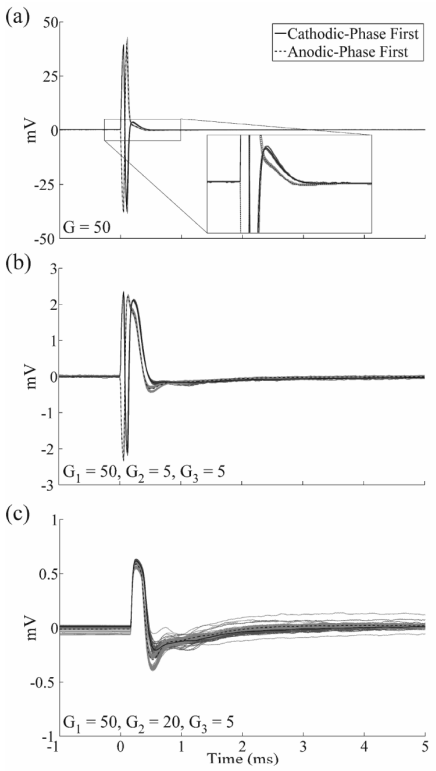

Figure 8.

The stimulus artefact and ECAP during *in vivo* recording using the monopolar symmetric configuration with the (a) conventional amplifier setup, (b) diodes-only instrumentation, and (c) complete DBS-ECAP instrumentation. The gains (G) used at the amplification stages of each recording system configuration are shown at the lower left of each graph. DBS was applied at time 0 with 3 V amplitude, 100 Hz frequency, and 50 μs pulse width, with both cathodic-phase first (solid traces) and anodic-phase first (dashed traces) polarities. The stimulus-triggered average waveform (black traces) and single trials (gray traces) are shown. The magnitudes of the recorded waveforms were gain-corrected.

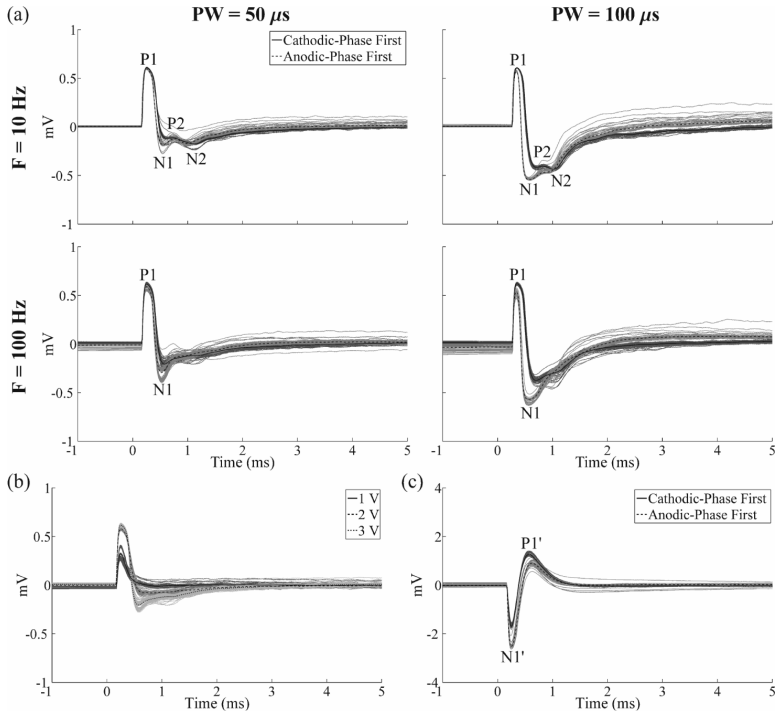

Figure 9.

Effect of stimulation parameters on the *in vivo* ECAP response recorded with the DBS-ECAP instrumentation. DBS was applied at time 0. (a) ECAPs recorded using the monopolar symmetric configuration across DBS pulse widths (PW) and frequencies (F) at a 3 V amplitude. The results for cathodic-phase first (solid traces) and anodic-phase first (dashed traces) polarities are shown. (b) ECAPs recorded using the monopolar symmetric configuration across DBS amplitudes at 100 Hz frequency and 50 μs pulse width, and with cathodic-phase first polarity. (c) ECAPs recorded using the monopolar asymmetric configuration with 3 V amplitude, 100 Hz frequency, and 50 μs pulse width. The results for cathodic- and anodic-phase first polarities are shown. For all figures, the stimulus-triggered average waveform (black traces) and single trials (gray traces) are shown. The magnitudes of the recorded waveforms were gain-corrected. The amplifier gains used for the monopolar symmetric and asymmetric configurations were 5,000 and 2,500, respectively.

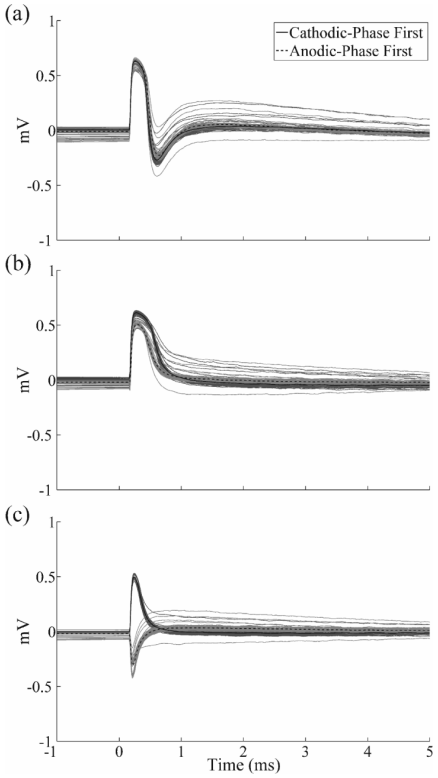

Figure 10.

Postmortem *in vivo* ECAPs at (a) 1 min, (b) 3 min, and (c) 5 min after euthanasia recorded with the DBS-ECAP instrumentation using the monopolar symmetric configuration. DBS was applied at time 0 with 3 V amplitude, 50 μs pulse width, 100 Hz frequency, and both cathodic-phase first (solid traces) and anodic-phase first (dashed traces) polarities. The stimulus-triggered average waveform (black traces) and single trials (gray traces) are shown. The magnitudes of the recorded waveforms were gain-corrected.

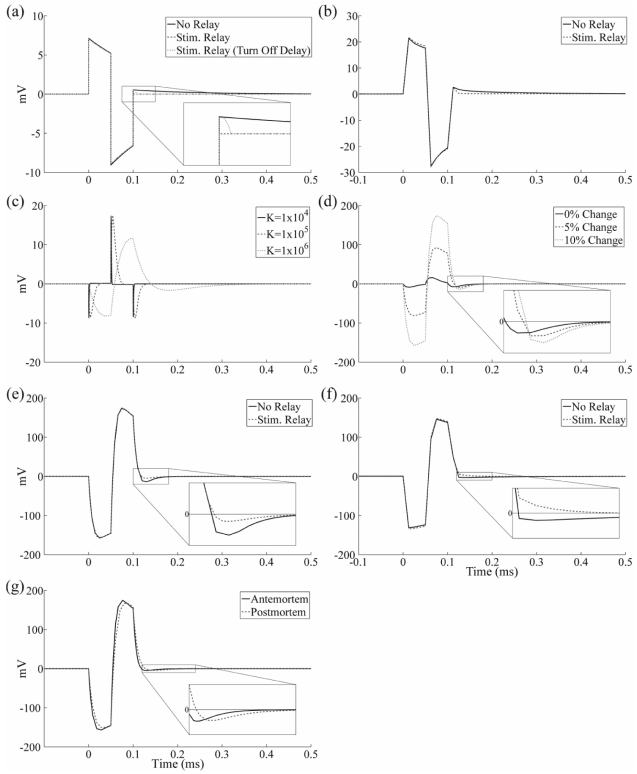

Figure 11.

Stimulus artefact waveforms calculated with the *in vitro* and *in vivo* electrical circuit equivalent models and comparison to experimentally recorded artefacts using the monopolar symmetric configuration. DBS was applied at time 0 with 3 V amplitude, 50 μs pulse width, 100 Hz frequency, and cathodic-phase first polarity. (a) *In vitro* circuit model artefacts calculated without the stimulator relay (solid trace), and with the relay either turned off immediately after the pulse (dashed trace) or with a 25 μs turn off delay (dotted trace). (b) Stimulus-triggered average artefact waveforms from the *in vitro* experiment recorded with a conventional amplifier without signal filtering, with the the stimulator relay absent (solid trace) and present (dashed trace). The magnitudes of the waveforms were gain corrected. (c) Sensitivity analysis of *in vivo* circuit model artefact to dielectric constant (K) values between 1×10^4 and 1×10^6. A dielectric constant of 3×10^5 was used for subsequent circuit model analysis. (d) Sensitivity analysis of *in vivo* circuit model artefact to changes in the bulk tissue resistance. The resistance was increased between contacts 0 and 1, and decreased between contacts 1 and 2, by the indicated value. A 10% bulk conductivity change was used for subsequent circuit model analysis. (e) *In vivo* circuit model artefacts calculated with and without the stimulator relay. (f) Stimulus-triggered average artefact waveforms from a postmortem *in vivo* cat experiment. Recordings were made with a conventional amplifier without signal filtering, both with and without the stimulator relay. A gain of 20 was used, and the magnitudes of the waveforms were gain corrected. (g) Comparison of circuit model artefact waveforms calculated using parameter values from the original, antemortem (solid trace) and postmortem (dashed trace) models. The stimulator relay was used for these data.

Table 1

Maximum gain (G) possible without saturation for the different recording system configurations and contact configurations tested *in vitro*. DBS was applied with 3 V amplitude, 50 μs pulse width, 100 Hz frequency, and cathodic-phase first polarity. The gain is also provided at each amplifier stage for recording system configurations with multiple stages.

Recording System	Monopolar Symmetric	Monopolar Asymmetric	Bipolar
Conventional Amplifier	**100**	**20**	**10**
Diodes-Only Instrumentation	**2,500** $G_1 = 100, G_2 = 5, G_3 = 5$	**500** $G_1 = 20, G_2 = 5, G_3 = 5$	**250** $G_1 = 10, G_2 = 5, G_3 = 5$
DBS-ECAP Instrumentation	**100,000** $G_1 = 100, G_2 = 200, G_3 = 5$	**40,000** $G_1 = 20, G_2 = 200, G_3 = 10$	**50,000** $G_1 = 10, G_2 = 500, G_3 = 10$

Table 2

Electrical circuit equivalent model parameters used for *in vitro* and *in vivo* models. The *in vivo* model used two sets of parameters to calculate the stimulus artefact in antemortem and postmortem recordings. The volume capacitance values shown for the *in vivo* models were calculated for dielectric constants of 3×10^5 and 2.92×10^5 for antemortem and postmortem, respectively. The resistance values of the volume conductor were calculated for conductivities of 0.3 and 0.216 S/m, respectively.

Parameter	In Vitro	In Vivo (Antemortem)	In Vivo (Postmortem)
Interface double-layer capacitance (C_{DL})	2.22 μF	1.56 μF	1.56 μF
Interface Faradaic resistance (R_F)	0.96 kΩ	1.50 kΩ	1.50 kΩ
Volume resistance between contacts 0 & 1 (R_{V01})	200.11 Ω	3208.69 Ω	4469.48 Ω
contacts 1 & 2 (R_{V12})	199.80 Ω	3270.33 Ω	4546.37 Ω
contact 0 & return (R_{V0})	127.26 Ω	2141.15 Ω	2980.29 Ω
contact 1 & return (R_{V1})	126.90 Ω	2184.88 Ω	3044.96 Ω
contact 2 & return (R_{V2})	128.34 Ω	2183.59 Ω	3071.81 Ω
Volume capacitance between contacts & return (C_V)	5.80 pF	9.38 nF	9.13 nF